

Improved Tissue Sodium Concentration Quantification in Breast Cancer by Reducing Partial Volume Effects – a Preliminary Study

Olgica Zaric^{1,2}, Carmen Leser³, Vladimir Juras⁴, Alex Farr³, Malina Gologan⁴, Stanislas Rapacchi^{5,6,7}, Laura Villazan Garcia¹, Christian Singer³, Siegfried Trattnig^{2,4}, Christian Licht^{8,9,10*}, Ramona Woitek^{1*}

¹Research Centre for Medical Imaging and Image Analysis (MIAAI), Danube Private University, Krems, Austria

²Institute for Musculoskeletal Imaging, Karl Landsteiner Society, St. Pölten, Austria

³Department for Gynecology and Obstetrics, Medical University of Vienna, Vienna, Austria

⁴High-field MR Centre, Medical University of Vienna, Vienna, Austria

⁵Department of Radiology, Lausanne University Hospital and University of Lausanne, Lausanne, Switzerland

⁶Aix-Marseille University, CNRS, CRMBM, Marseille, France

⁷APHM, Hôpital Universitaire Timone, CEMEREM, Marseille, France

⁸Radiological Sciences Laboratory, School of Medicine, Stanford University, Stanford, California, USA

⁹Computer Assisted Clinical Medicine, Medical Faculty Mannheim, Heidelberg University, Mannheim, Germany

¹⁰Mannheim Institute for Intelligent Systems in Medicine, Medical Faculty Mannheim, Germany

*Authors equally contributed to this manuscript

**Corresponding author: Olgica Zaric

E-mail: olgica.zaric@dp-uni.ac.at

Address: Research Centre for Medical Imaging and Image Analysis (MIAAI), Danube Private University (DPU), Viktor Kaplan-Straße 2, 2700 Wiener Neustadt, Austria

Abstract:

Introduction: In sodium (^{23}Na) MRI, partial volume effects (PVE) are one of the most common causes of errors in the quantification of tissue sodium concentration (TSC) *in vivo*. Advanced image reconstruction algorithms, such as compressed sensing (CS) have been shown to potentially reduce PVE. Therefore, we investigated the feasibility of CS-based methods for image quality and TSC quantification accuracy improvement in patients with breast cancer (BC).

Subjects and Methods: Three healthy participants and 12 female participants with BC were examined on a 7T MRI scanner in this study. We reconstructed ^{23}Na -MRI images using the weighted total variation (wTV) and directional total variation (dTV), anatomically guided total variation (AG-TV) and, adaptive combine (ADC) reconstruction and performed image quality assessment. We evaluated agreement in tumor volumes delineated on sodium data using the Dice score and performed TSC quantification for different image reconstruction approaches.

Results: All methods provided sodium images of the breast with good quality. The mean Dice scores for wTV, dTV and AG-TV were $65\pm 11\%$, $72\pm 9\%$ and $75\pm 6\%$, respectively. In the breast tumors, average TSC values were 83.0 ± 4.0 (72.0 ± 5.0) mmol/L, 80.0 ± 5.0 mmol/L, and 84.0 ± 5.0 mmol/L, respectively. There was a significant difference between dTV and wTV ($p<0.001$), as well as between dTV and AG-TV ($p<0.001$), and dTV and ADC algorithm ($p<0.001$).

Conclusion: The results of this study showed that there are differences in tumor appearance and TSC estimations that might be depending on the type of image reconstruction and parameters used, most likely due to differences in their robustness in reducing PVE.

Key words: sodium magnetic resonance imaging; tissue sodium concentration; breast cancer; partial volume effects; compressed sensing; image reconstruction

Abbreviations:

AC, adaptive combine

AG-TV, anatomically guided total variation

B_0 , static magnetic field

BC, breast cancer

B_1 , combined transmit and receive radiofrequency field

B_1^+ , transmit radiofrequency field

CS, compressed sensing

dTV, directional total variation

PVE, partial volume effect

SNR, signal to noise ratio

TSC, tissue sodium concentration

wTV, weighted total variation

Highlights:

- TSC is one of the most promising imaging markers for breast tumor diagnosis.
- PVE may have a substantial impact on TSC quantification.
- Reducing the PVE in ^{23}Na -MRI involves using advanced image reconstruction methods.

1 Introduction

Sodium magnetic resonance imaging (^{23}Na -MRI) may noninvasively provide biochemical information on cell viability, structural integrity, and energy metabolism, and therefore, enables assessment of pathophysiological changes in human tissue [1, 2]. The quantitative parameter derived from ^{23}Na -MRI data, tissue sodium concentration (TSC), is one of the most promising imaging markers for breast tumor identification and treatment response evaluation [3-7].

Partial volume effects (PVE) may have a substantial impact on TSC quantification accuracy due to the low nominal resolution (the most common voxel size is $(3\text{ mm})^3$) used for ^{23}Na -MRI [8]. In addition, the non-Cartesian three-dimensional density-adapted radial (DA-3DPR) sequence enables measurements with ultra-short echo time (UTE), which is particularly beneficial for increasing signal-to-noise ratio (SNR) and reducing $T2^*$ sensitivity to allow more accurate TSC quantification. Unfortunately, DA-3DPR yields a large full width half maximum (FWHM) of the corresponding point spread function (PSF), which further increases PVE [9]. Since this sequence is currently widely used in clinical research studies, the influence of PVE on TSC values must be considered. As was demonstrated by Lott et al. when measuring cardiac TSC, the PVE contribution is the largest [10]; similarly, Zaric et al. showed that errors due to PVE contribute 25-30% to an overall TSC quantification error in breast tumors [5], further showcasing the need for in-depth investigation of the introduced bias of PVE in TSC estimations.

Besides PVE correction algorithms that incorporate anatomical information to better delineate tissue boundaries and correct for the effects of voxel averaging [11, 12], advanced image reconstruction methods, such as compressed sensing (CS), may enhance image quality in terms of SNR and better tissue differentiation [13], as well as algorithms based on high-resolution and low-noise structural prior (anatomical) images [14, 15]. Substantial improvements were noticeable with an introduction of the CS concept to sodium MRI by using

a proton support region constraint [14], and further advanced it by adding an edge-weighting-based constraint to exploit proton anatomical information [15].

Lachner et al. demonstrated that including structural prior information from various proton MR contrasts using an anatomically weighted first- and second-order total variation (AnaWeTV) leads to significantly increased SNR and enhanced resolution of known structures in the images [16, 17]. Zhao et al. proposed a reconstruction method based on a motion-compensated generalized series model and a sparse model where prior anatomical information from a segmented high-resolution proton image was used for denoising and resolution enhancement. The authors also concluded that the proposed anatomically constrained reconstruction method substantially improved SNR and lesion fidelity [18].

Ehrhardt et al. proposed image reconstruction using anatomical guidance based on the segmentation-free directional total variation (dTV) prior anatomical structure knowledge not only for denoising and resolution enhancement of ^{23}Na images, but also for local signal decay [19] estimation and compensation in a joint reconstruction framework for dual-echo ^{23}Na acquisitions [20].

Subsequently, Licht et al. developed a method for a reconstruction framework that addresses the shortcomings of ^{23}Na multi-quantum coherence imaging by utilizing ^1H prior constraints, taking into account the signal from different structures rather than prior anatomical information [21]. These reconstruction methods were shown to be robust in increasing overall image quality and in reducing PVE, which may help in increasing the accuracy of TSC quantification [22].

The above-mentioned methods have great potential for image quality enhancement in terms of SNR, fine tissue structural delineation, and lesion conspicuity, as well as for reducing the PVE, and thus, we aimed to investigate the feasibility of methods proposed by Ehrhardt et al. [19] (method#1) and Licht et al. [21] (method#2) to attempt to achieve improvements in the accuracy of TSC quantification. In addition, we aimed to compare these two methods with TSC

values derived from ^{23}Na -MR images reconstructed with an adaptive combined (ADC) method [23] (method#3) in patients with breast cancer (BC).

2 Materials and Methods

2.1 Calibration probes and calibration phantom

Two vials made of saline solution (NaCl) with a sodium concentration of 77 mmol/L and 154 mmol/L mixed with 4% agarose gel (Agarose, Sigma-Aldrich, USA) were prepared just before the study was started and were attached to the inner parts of both breast coil elements. To match T_1 relaxation times properties of the breast tissue, we added 2.9 g/L copper sulfate to the mixture.

A simulation phantom was created that assigned TSC values of 40 mmol/L to the glandular tissue, 20 mmol/L to the adipose tissue and 77 mmol/L and 154 mmol/L to the prepared vials. The phantom served as a dual reference for reading signal intensities from glandular and adipose tissue and for evaluating the accuracy of vial concentrations and vice versa for the two tissue types.

2.2 Study participants

Three healthy female subjects and 12 women with breast cancer were enrolled in this study. All MRI exams were performed between January 2023 and March 2024 in collaboration with Medical University of Vienna and were approved by the local research ethics committee (ethics approval number: 1131/2015, cooperation agreement number: 2023-030). Written, informed consent was obtained from all participants in the study. All methods were performed following the Declaration of Helsinki.

2.3 MR Imaging

MRI was performed on a whole-body 7.0 T MR scanner with a 70 mT/m gradient amplitude and a 200 mT/m/ms slew rate (Magnetom Dot Plus, Siemens Healthineers, Germany).

All participants were measured in the prone position. A Tx/Rx dual-tuned sodium and proton (^{23}Na and ^1H) bilateral breast coil (14 ^{23}Na channels and two ^1H channels; QED) was used. ^{23}Na MRI data sets were acquired using a density-adapted, three-dimensional radial projection reconstruction (3D DA-PR) pulse sequence [9]. The sequence parameters for a nominal spatial resolution of 3 mm^3 was as follows: repetition time msec/echo time msec, 100/0.55; pulse duration, 1 msec; nominal flip angle, 90° calibrated for the maximum signal intensity; readout time, 10.02 msec; bandwidth of 100 Hz/px; and acquisition time, 16 min. The number of projections was 8000, with 384 radial samples per projection. Sodium imaging was followed by noise-only scans (no radio frequency [RF] power). Morphologic, proton (^1H) three-dimensional double-echo steady state sequence (3D DESS) [24], and images were acquired with the following parameters: field of view, $320\times 320\text{ mm}^2$; nominal resolution, $(1\text{ mm})^3$; 9.3/2.6, (repetition time msec/echo times msec); and acquisition time, 2 min and 30 seconds. The total scanning time of this study was around 20 minutes.

2.4 Breast tissue and tumor segmentation

Segmentation masks of different tissues were created based on high-resolution ^1H DESS images. In healthy subjects, glandular and adipose tissue and vials (77 mmol/L and 154 mmol/L) were labeled as four different compartments. In patients, the whole breast, tumor, and calibration phantoms were segmented manually by an MRI physicist and a biomedical engineer using ITK-SNAP software (version 4.0.0) supervised by a subspecialty trained breast radiologist. Since the high-resolution morphological ^1H MR imaging was performed at 7T without any contrast medium, we used 3T data for precise lesion location and verification of margins. The same segmentation mask was applied on the ^{23}Na -MRI images reconstructed by different methods.

2.5 Image reconstruction

^{23}Na MRI were reconstructed offline using custom-written scripts in Matlab software (version R2022a; MathWorks).

2.5.1 Method#1: Weighted Total Variation (wTV) and Directional Total Variation (dTV)

Ehrhardt et al. proposed a method of two modifications of total variation (TV) incorporating structural knowledge taking *a priori* information on i) location of edges (weighted total variation (wTV)) and ii) direction of edges (directional total variation (dTV)) into account and reduce the total variation in the degenerate case when no knowledge on tissue structure is available. For solving convex optimization problem alternating direction method of multipliers (ADMM) was used:

$$\operatorname{argmin}_{u \in [0, \infty)^N} \{ \frac{1}{2} \|A_u - b\|^2 + \alpha J(u) \} \quad (1)$$

where $A: \mathbb{R}^N \rightarrow \mathbb{C}^M$ is the MRI forward operator, b the acquired data, and $u \in [0, \infty)^N \subset \mathbb{R}^N$ is object of interest sampled from MRI data. ADMM separates the forward operator from the prior. For both priors, the corresponding proximal operator can be implemented as an extension of the fast gradient projection method on the dual problem for total variation. Ultimately, the goal of this method is not only to obtain better defined images but also to improve the reconstruction of smooth structures and fine details. The reconstruction algorithms used in this paper are available as supplementary material (M104732 01.zip[local/web 6.50 MB]) [19].

2.5.2 Method#2: Anatomically Guided Total Variation (AG-TV)

The second method tried to synthesize the missing high-frequency components of the k-space with constraints from the ^1H image. Therefore, the ^{23}Na images were processed to limit PVE with constraints from the ^1H prior first-order total variation model:

$$\min_u \lambda_{x,y,z} \|\nabla_x u, \nabla_y u, \nabla_z u\|_2 + \lambda_{BM} \|BM * u\|_2 \text{ s. t. } \|\Phi_F(u) - f\|_2^2 < \sigma^2 \quad (2)$$

with u being the targeted improved interpolated image, Φ_F representing the Fourier sampling operator, f the measured data in k-space, and σ^2 being the signal variance noise. ^1H prior information was used to detect sharp edges by calculating the first derivative along x, y, and z of the high-resolution ^1H image. The derivatives were inverted and can be regarded as

threshold maps to locally enhance edges and support TV denoising. The amount of included prior information can be controlled by setting a threshold, ω , similar to [15]. $\lambda_{BM} \|BM * u\|_2$ represents another regularization term that penalizes the area outside the region of interest, e.g., air to further reduce partial volume effects. BM is a binary mask that allows selection of the background area. The Split-Bregman was utilized to solve the optimization problem stated in equation 2 with the following empirically determined weighting factors: $\lambda_{x,y,z} = \lambda_{BM} = 1$ [16].

2.5.3 Method#3: Adaptive Combine (ADC) reconstruction

^{23}Na -MR images reconstructed utilizing an adaptive combined (ADC) approach served as ground-truth [23]. The images were not corrected for B_0 and B_1^+ inhomogeneity and served as ground-truth for method#1 and method#2.

2.6 Image quality assessments

We used Dice score for a comparison of tumor volumes segmented on sodium images. We analyzed the signal intensity profiles through a regular structure in each patient, as the signal intensity distribution (ImageJ, LOCI, University of Wisconsin, USA) is determined by the point spread function (PSF), which determines the level of detail and sharpness in the image. The structural similarity index (SSIM) and root mean square error (RMSE) were used for image quality assessments [25] and focus measure (FM), a “variation of the Laplacian” [26], to determine whether reconstructed images were less blurred compared to sodium images reconstructed with ADC approach (method#3).

2.7 Tumor TSC quantification

The signal intensities of the calibration solutions obtained from the ^{23}Na images reconstructed using method#1, method#2, and method#3 were fitted linearly to a two-point calibration curve [27]. For each segmentation region, the signals were automatically provided by the software. Sodium signals from the vials were used for a calibration curve derivation and determination of tumor TSC values. The approach assumed that the water concentration was

the same in standards (100%) and tissue (~75%); therefore, the correction factor of 0.75 for the lower water content of tissue was applied to avoid underestimation of TSC in breast tumors [8].

2.8 Statistical tests

Statistical analysis of the data was performed using SPSS software for Windows (IBM SPSS Statistics, version 30.0, Armonk, NY). Metric data are described by means (mean±SD) and normal distribution of measured values was tested using the Shapiro Wilks test. For categorical data, absolute frequencies and percentages were presented. The relationship between image metrics and TSC values for different algorithms were analyzed using the paired samples test and, for agreement in TSC of the phantoms, we used the Pearson correlation test. A *p* value smaller than 0.05 was considered significant.

3 Results

The mean age of three healthy subject was (mean ± SD) 40.0±8.0 years and 55.0±14.0 years for the subjects with cancers. All data showed a normal distribution. Eleven participants were diagnosed with invasive ductal carcinoma (IDC) and one with invasive lobular carcinoma (ILC). The mean one-dimensional tumor size was 16±8 mm. In patients with more than one tumor, we included the larger sized one in this analysis. More details on demographic data of the study participants with breast tumors may be found in Table 1.

3.1 Image quality evaluation

Images demonstrated that method#1 and method#2 provided images with good image quality that retained sodium signal intensities and tissue structures well (Figure 1 (a-l), Figure 2 (a-l), Figure 3 (a-l)). However, lesion conspicuity was not the same for images reconstructed using wTV, dTV and AG-TV. For method#1, the tumor margins were better visualized with increasing number of projections; differences in lesion volume and shape were observed compared to proton images. When comparing tumor segmentation of ground truth images with method#1, we found a Dice score of 65±11% for wTV and 72±6% and for dTV. The same

comparison gave a Dice score of 75±% for AG-TV. When we analyzed the signal intensity profile through the tumor, we found differences in their values and shapes (Figure 4 (a-j)).

The mean±SD of quantitative parameters (SSIM, RMSE, and FM) for two methods were calculated for 20 slices for each patient. Method#1 demonstrated that increasing the number of radial projections from 8 to 64 improved image quality. For 64 radial projections method#1 (wTV), SSIM was 0.39±0.02, RMSE was 45.60±5.0, and FM was 46.6±9.0. For the same parameters, the dTV method provided the following values: RMSE was 45.5±4.0; SSIM was 0.39±0.02; and FM was 62.2±4.0. When SSIM between wTV and dTV were compared, we found no significant difference for each number of projections: for 8 projections p=0.904; for 16 projections, p=0.380; and p=0.342 and p=0.228 for 32 and 64 projections, respectively (Figure 5 (a, b)). There were similar findings for RMSE: p=0.530, p=0.065, p=0.865, and p=0.964, for 8, 16, 32, and 64 projections, respectively (Figure 5 (c, d)).

However, when we compared the average focus measure between wTV vs dTV, we found significant differences for the FM: p<0.001, p<0.001, p<0.001 for 8, 16, 32, and 64 projections, respectively (Figure 5 (e, f)). For AG-TV, changing parameters such as number of iterations did not influence image quality metrics. SSIM, RMSE, and FM were 0.40±0.04, 41.6±5.0, and 30.0±4.0, respectively. For method#3, the FM was 26.3±5.0 and was 43.5%, lower compared to wTV (64 projections), 57.9% for dTV (64 projections), and 12.3% lower compared to AG-TV. When dTV vs AG-TV was compared in terms of SSIM, RMSE, and FM, the differences were as follows: p=0.472, p=0.004, and p<0.001, respectively (Figure 6 a-c).

3.2 TSC quantitative evaluations

3.2.1 Phantom measurements

TSC value for the phantoms with known concentrations of 77.0 mmol/L and 154.0 mmol/l were calculated using all three methods and were as follows: for wTV (dTV) TSC were 88.0±12.0 (80.0±6.0) mmol/L for 77 mmol/L and 162.0±11.0 (159.0±9.0) mmol/L for 154.0 mmol/L, respectively. For AG-TV, these values were 88.0±10.0 mmol/L and 168.0±7.0

mmol/L, and for ADC the values were 89.0 ± 5.0 mmol/L and 165.0 ± 10.0 mmol/L. When we correlated measured sodium concentrations with prepared concentrations, we found high correlation coefficients, albeit not significant: $r=0.791$; $p=0.169$ for wTV, $r=0.885$; $p=0.076$ for dTV, $r=0.830$; $p=0.241$ for AG-TV, and $r=0.812$; $p=0.155$ for ADC reconstruction.

3.2.2 *In vivo* measurements

TSC of healthy glandular tissue was 58.0 ± 6.0 (50.0 ± 4.0) mmol/L, 52.0 ± 5.0 mmol/L, 54.0 ± 8.0 mmol/L, 56.0 ± 6.0 mmol/L and, in tumors 83.0 ± 4.0 mmol/L, 72.0 ± 4.0 mmol/L, 80.0 ± 5.0 mmol/L, and 84.0 ± 5.0 mmol/L evaluated by wTV, dTV, AG-TV, and ADC, respectively. Comparing the TSC found in tumors between dTV vs AG-TV ($p < 0.001$), dTV vs ADC ($p < 0.001$), and AG-TV vs ADC ($p < 0.001$), we found significant differences between them (Table 2).

4 Discussion

In this study, we implemented and investigated the feasibility of the methods proposed by Ehrhardt et al. (method#1) and Licht et al. (method#2) to evaluate image quality and TSC quantification accuracy in breast tissue. As a standard method, we used ^{23}Na -MR images reconstructed using an adaptive combine algorithm (method#3).

It has been shown that image quality in general and the availability of high-quality multi-parametric MRI data providing detailed insights into tumor characteristics might be crucial for accurate tumor delineation [28, 29]. Newly applied methods for ^{23}Na -MRI data reconstruction in breast cancer patients provided good image quality. Nevertheless, we found remarkable discrepancies when comparing tumor features (shape and volume) on wTV, dTV and AG-TV reconstructed images with ground truth images (ADC reconstruction). Moderate values of the Dice score showed a different robustness of the methods in the faithful representation of the tumor margins. The image reconstruction methods showed large differences in the image quality of the data, i.e., recognizable deviations in the representation of small morphological details, inconsistencies in the tumor borders, the visibility of the skin, etc. These results show

that the fidelity in visualizing tissue structures depends on the image reconstruction method and can be strongly influenced by its selection. When we analyzed signal intensities through tissue structures, as an estimation of point spread functions (PSFs), we found that they vary considerably depending on the reconstruction method used.

The image quality metrics, such as SSIM, did not show a substantial disagreement between two methods, while the largest differences in RMSE and FM were found for dTV vs AG-TV. Three image reconstruction methods were applied on BC patients' data sets, and when the method by Ehrhardt et al. (dTV) was compared to the method by Licht et al. (AG-TV) and the standard approach (ADC reconstruction), we demonstrated significant differences in TSC values found in malignant breast tumors ($p < 0.001$; $p < 0.001$; $p < 0.001$), respectively.

CS in ^{23}Na -MRI has been demonstrated as a method with a high potential in reducing scanning time and improving image quality [13]; nevertheless, the method was considered to introduce a bias in the quantitative assessment of imaging with low SNR, such as ^{23}Na -MRI. However, an investigation of CS effects on image quality and TSC quantification accuracy in the human brain showed that wavelet-based CS reconstructions provide the highest image quality with stable TSC estimates for most undersampling factors [30]. In the muscle, 3D dictionary-learning compressed sensing enables accelerated quantification with a high accuracy [31, 32].

Using a method based on CS and proposed by Erhardt et al., we found that exploiting the two-dimensional directional information results in images with well-defined edges, superior to those reconstructed solely using *a priori* information about the edge location. When method#1 was compared to method#2, the quantitative image metrics, SSIM, did not indicate substantial disagreement; yet visual inspection revealed an increased image quality for the method by Licht et al., especially in the fine delineation of glandular tissue structures. Sodium images reconstructed by method#2 showed a higher level of noise as did the ground-truth

images, which was detected by the similarity measures while being filtered out by human visual assessment.

Although the improvement in image quality was evident in terms of blurring, noise, and delineation of fine structural details by introducing CS-based algorithms for data reconstruction [16, 17], the impact of image quality on TSC was not fully investigated. In our study, we showed that image quality metrics may indicate the existence of a difference in TSCs. However, the proton anatomical information that is not contained in the sodium dataset can introduce artificial structures to the reconstructed sodium images. If these structures contain a significant amount of sodium, such as glandular tissue, the TSC will be unrealistically increased. Thus, it is critical that only reliable prior information is used for the anatomical incorporation, such as well-defined surrounding breast glandular and tumor tissue [18].

Our results demonstrated that the dTV method has the highest accuracy when TSC was measured in phantoms. *In vivo*, TSC of glandular tissue was higher for all methods compared to literature values [4, 33, 34]. In carcinomas, TSCs were also elevated compared to those reported in the literature [3-5, 35]. There are two potential reasons for this: first, glandular tissue, as well as cancers, are rich in fine structures that enhance the TV (sum of the gradients) and increase TSC, as the extent of denoising varies greatly in these structures. Second, the TSC quantification pipeline did not include B_0 and B_1^+ inhomogeneity corrections and, as reported earlier, the contribution of these two factors is relatively small compared to PVE errors ($\sim 10\%$ for B_0 and B_1^+ together [5, 10]), but increases when reconstructions are iteratively performed and thus, non-linear. However, including these corrections in the quantification pipeline might further increase accuracy and reduce a bias in TSC quantification.

The main limitation of this study is the small number of patients and the nonexistent literature data on actual sodium concentration in tumor tissue obtained with a non-imaging method. We also believe that the methods developed by Schramm et al. might improve the

accuracy of TSC quantification and future investigations might address this research question [20].

5 Conclusion

Reducing the partial volume effects in ^{23}Na -MR imaging involves using advanced image reconstruction methods that enhance image quality, increase SNR, and refine tissue boundaries. Different image reconstruction methods may contribute to mitigating PVE by addressing the voxel-mixing issue, thereby improving the accuracy of tissue differentiation based on quantitative TSC evaluations. By tailoring the reconstruction approach to the imaging modality and clinical need, it is possible to minimize the impact of PVE and enhance image quality and TSC quantification accuracy.

References:

1. Zaric, O., et al., *Frontiers of Sodium MRI Revisited: From Cartilage to Brain Imaging*. J Magn Reson Imaging, 2021. **54**(1): p. 58-75.
2. Thulborn, K.R., *Quantitative sodium MR imaging: A review of its evolving role in medicine*. Neuroimage, 2018. **168**: p. 250-268.
3. Ouwerkerk, R., et al., *Elevated tissue sodium concentration in malignant breast lesions detected with non-invasive ^{23}Na MRI*. Breast Cancer Res Treat, 2007. **106**(2): p. 151-60.
4. Zaric, O., et al., *Quantitative Sodium MR Imaging at 7 T: Initial Results and Comparison with Diffusion-weighted Imaging in Patients with Breast Tumors*. Radiology, 2016. **280**(1): p. 39-48.
5. Zaric, O., et al., *Tissue Sodium Concentration Quantification at 7.0-T MRI as an Early Marker for Chemotherapy Response in Breast Cancer: A Feasibility Study*. Radiology, 2021. **299**(1): p. 63-72.
6. James, A.D., et al., *Sodium accumulation in breast cancer predicts malignancy and treatment response*. Br J Cancer, 2022. **127**(2): p. 337-349.
7. Poku, L.O., et al., *(^{23}Na) MRI as a Noninvasive Biomarker for Cancer Diagnosis and Prognosis*. J Magn Reson Imaging, 2021. **53**(4): p. 995-1014.
8. Gast, L.V., et al., *Recent technical developments and clinical research applications of sodium (^{23}Na) MRI*. Prog Nucl Magn Reson Spectrosc, 2023. **138-139**: p. 1-51.
9. Nagel, A.M., et al., *Sodium MRI using a density-adapted 3D radial acquisition technique*. Magn Reson Med, 2009. **62**(6): p. 1565-73.
10. Lott, J., et al., *Corrections of myocardial tissue sodium concentration measurements in human cardiac (^{23}Na) MRI at 7 Tesla*. Magn Reson Med, 2019. **82**(1): p. 159-173.
11. Niesporek, S.C., et al., *Partial volume correction for in vivo (^{23}Na) MRI data of the human brain*. Neuroimage, 2015. **112**: p. 353-363.

12. Kim, S.Y., et al., *Voxel-wise partial volume correction method for accurate estimation of tissue sodium concentration in (23) Na-MRI at 7 T*. NMR Biomed, 2021. **34**(2): p. e4448.
13. Chen, Q., N.J. Shah, and W.A. Worthoff, *Compressed Sensing in Sodium Magnetic Resonance Imaging: Techniques, Applications, and Future Prospects*. J Magn Reson Imaging, 2022. **55**(5): p. 1340-1356.
14. Gnahn, C., et al., *Iterative 3D projection reconstruction of (23) Na data with an (1) H MRI constraint*. Magn Reson Med, 2014. **71**(5): p. 1720-32.
15. Gnahn, C. and A.M. Nagel, *Anatomically weighted second-order total variation reconstruction of 23Na MRI using prior information from 1H MRI*. Neuroimage, 2015. **105**: p. 452-61.
16. Lachner, S., et al., *Compressed sensing and the use of phased array coils in (23)Na MRI: a comparison of a SENSE-based and an individually combined multi-channel reconstruction*. Z Med Phys, 2021. **31**(1): p. 48-57.
17. Lachner, S., et al., *Compressed sensing reconstruction of 7 Tesla (23)Na multi-channel breast data using (1)H MRI constraint*. Magn Reson Imaging, 2019. **60**: p. 145-156.
18. Zhao, Y., et al., *High-resolution sodium imaging using anatomical and sparsity constraints for denoising and recovery of novel features*. Magn Reson Med, 2021. **86**(2): p. 625-636.
19. Ehrhardt, M.J.B., M.M., *Multicontrast MRI Reconstruction with Structure-Guided Total Variation*. SIAM J. IMAGING SCIENCES, 2016. **9**(3): p. 1084-1106.
20. Schramm, G., et al., *Resolution enhancement, noise suppression, and joint T2* decay estimation in dual-echo sodium-23 MR imaging using anatomically guided reconstruction*. Magn Reson Med, 2024. **91**(4): p. 1404-1418.
21. Licht, C., et al., *Multidimensional compressed sensing to advance (23) Na multi-quantum coherences MRI*. Magn Reson Med, 2023.

22. Christian Licht, L.R.S., Stanislas Rapacchi, *An iterative algorithm for resolving high-resolution ^{23}Na Multi-Quantum Coherences MRI from prior ^1H constraints*, in *ISMRM*. 2022: London, UK.
23. Walsh, D.O., A.F. Gmitro, and M.W. Marcellin, *Adaptive reconstruction of phased array MR imagery*. *Magn Reson Med*, 2000. **43**(5): p. 682-90.
24. Bruder, H., et al., *A new steady-state imaging sequence for simultaneous acquisition of two MR images with clearly different contrasts*. *Magn Reson Med*, 1988. **7**(1): p. 35-42.
25. Mason, A., et al., *Comparison of Objective Image Quality Metrics to Expert Radiologists' Scoring of Diagnostic Quality of MR Images*. *IEEE Trans Med Imaging*, 2020. **39**(4): p. 1064-1072.
26. Rajevenceltha, J. and V.H. Gaidhane, *A novel approach for image focus measure*. *Signal, Image and Video Processing*, 2021. **15**(3): p. 547-555.
27. Lu, A., et al., *Quantitative sodium imaging with a flexible twisted projection pulse sequence*. *Magn Reson Med*, 2010. **63**(6): p. 1583-93.
28. Larkin, J.R., et al., *Improving Delineation of True Tumor Volume With Multimodal MRI in a Rat Model of Brain Metastasis*. *Int J Radiat Oncol Biol Phys*, 2020. **106**(5): p. 1028-1038.
29. Kataoka, M., et al., *Multiparametric Approach to Breast Cancer With Emphasis on Magnetic Resonance Imaging in the Era of Personalized Breast Cancer Treatment*. *Invest Radiol*, 2024. **59**(1): p. 26-37.
30. Blunck, Y., et al., *Compressed sensing effects on quantitative analysis of undersampled human brain sodium MRI*. *Magn Reson Med*, 2020. **83**(3): p. 1025-1033.
31. Utschneider, M., et al., *Accelerated quantification of tissue sodium concentration in skeletal muscle tissue: quantitative capability of dictionary learning compressed sensing*. *MAGMA*, 2020. **33**(4): p. 495-505.

32. Utschneider, M., et al., *Towards accelerated quantitative sodium MRI at 7 T in the skeletal muscle: Comparison of anisotropic acquisition- and compressed sensing techniques*. Magn Reson Imaging, 2021. **75**: p. 72-88.
33. Arponen, O., et al., *(23)Na MRI: inter-reader reproducibility of normal fibroglandular sodium concentration measurements at 3 T*. Eur Radiol Exp, 2024. **8**(1): p. 75.
34. Arponen, O., et al., *23Na MRI: inter-reader reproducibility of normal fibroglandular sodium concentration measurements at 3 T*. European Radiology Experimental, 2024. **8**(1): p. 75.
35. Jacobs, M.A., et al., *Monitoring of neoadjuvant chemotherapy using multiparametric, (2)(3)Na sodium MR, and multimodality (PET/CT/MRI) imaging in locally advanced breast cancer*. Breast Cancer Res Treat, 2011. **128**(1): p. 119-26.

Table 1: Demographic features of participants of the study

Subject No.	Age (years)	BIRADS	Menopause status	Tumor size (mm)	Verification	Histologic type	Grade
1	43	/	Pre	/	/	/	/
2	38	/	Pre	/	/	/	/
3	39	/	Pre	/	/	/	/
4	40	5	Pre	12	Biopsy	IDC	2
5	59	5	Post	35	Biopsy	IDC	3
6	58	4	Post	9	Biopsy	IDC	1
7	29	5	Pre	19	Biopsy	IDC	2
8	59	5	Post	15	Biopsy	IDC	2
9	71	2	Post	9	Biopsy	IDC	2
10	46	4	Pre	18	Biopsy	IDC	2
11	38	5	Pre	18	Biopsy	IDC	3
12	65	5	Post	26	Biopsy	IDC	3
13	72	4	Post	5	Biopsy	IDC	2
14	46	4	Post	20	Biopsy	IDC	3
15	71	4	Post	11	Biopsy	ILC	2

Table 2: Results of paired samples test for paired differences in tissue sodium concentrations (TSC) in breast cancer patients calculated using three different image reconstruction methods

Pair	Mean	Standard deviation	95% Confidence Interval of the Difference		Significance Two-Sided p
			Lower	Upper	
wTV - dTV	10.72	4.20	8.05	13.38	<0.001
wTV - AG-TV	2.83	4.16	0.190	5.48	0.038
dTV - AG-TV	7.88	3.18	5.86	9.90	<0.001
wTV - ADC	-0.65	3.75	-3.04	1.74	0.581
dTV - ADC	11.37	4.71	8.37	14.36	<0.001
AG-TV - ADC	3.48	2.18	2.10	4.86	<0.001

* wTV: weighted total variation; dTV: structure guided total variation; AG-TV: anatomically guided total variation

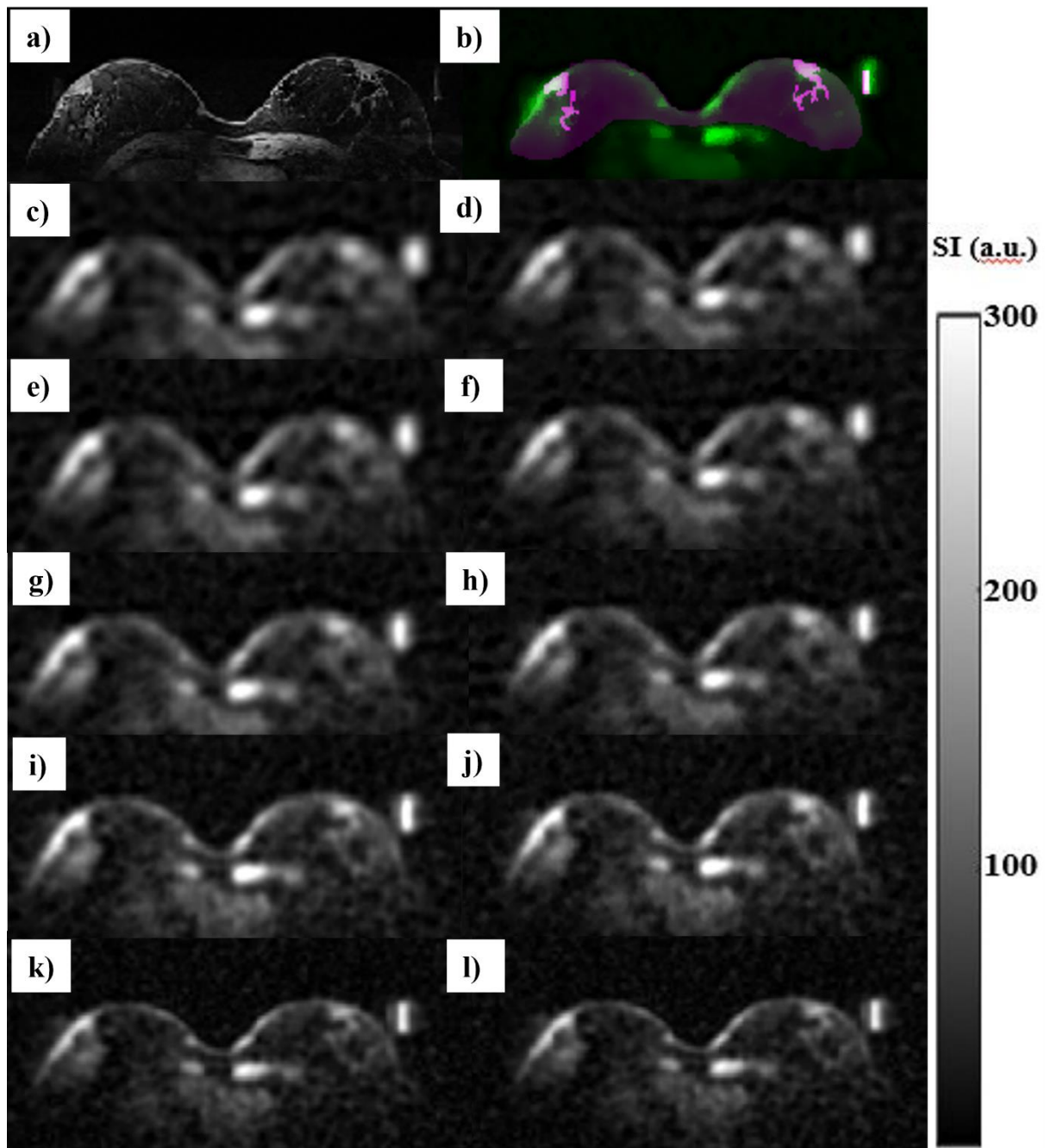


Figure 1: The figure demonstrates MR images of a 44-year-old healthy female subject (#1), a) proton DESS image in axial orientation, b) segmentation mask of breast, a sodium (^{23}Na) MR image reconstructed using wTV method for c) 8 projections, g) 16, e) 32, and i) 64 radial projections and dTV for d) 8 projections, f) 16, k) 32, and j) 64 radial projections. k) show the image reconstructed using AG-TV and a l) ground truth sodium image (ADC reconstruction). Gray-scale bar shows image signal intensity (SI) in arbitrary units (a.u.)

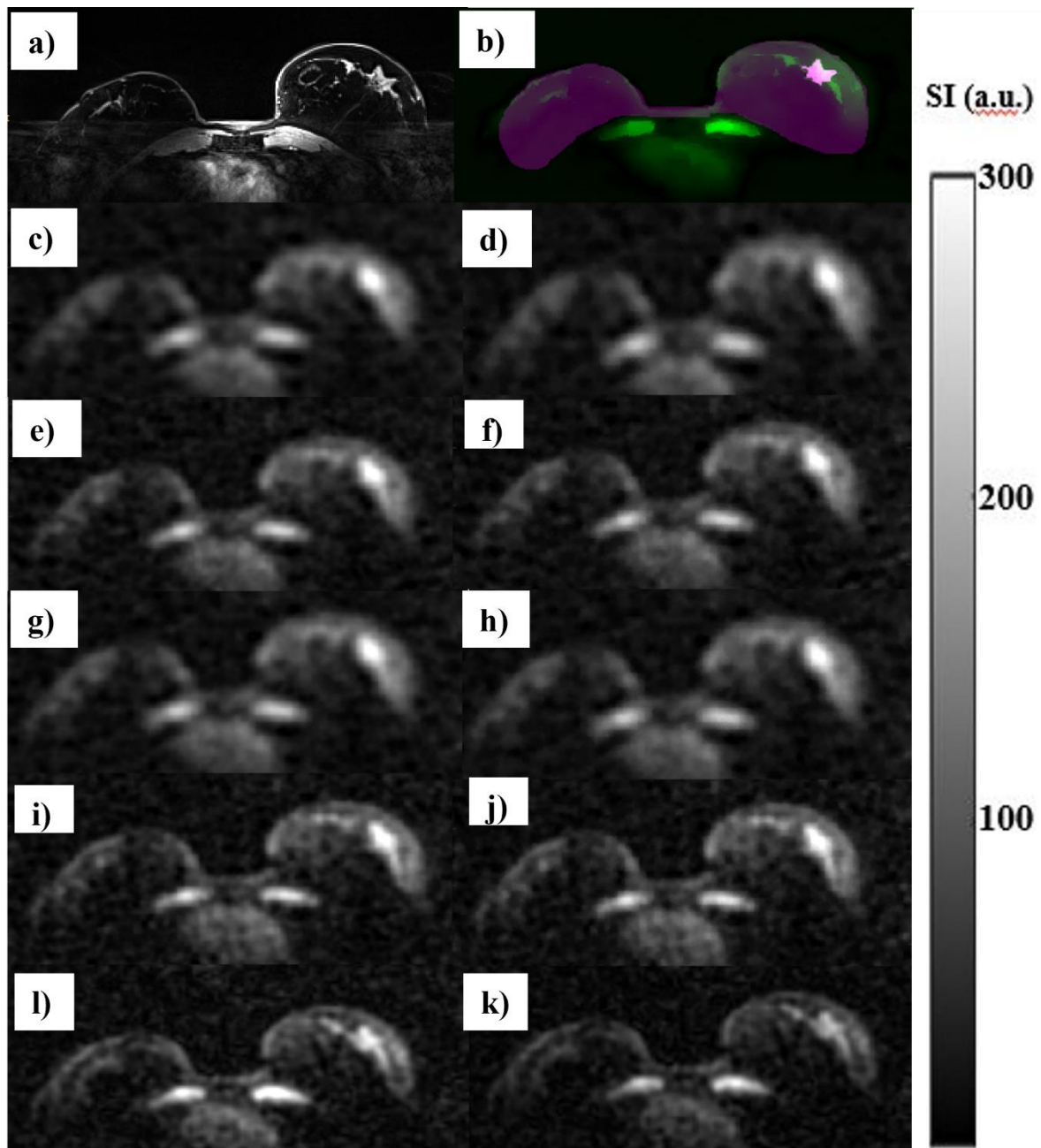


Figure 2: A 46-year-old female subject (#10) with invasive ductal carcinoma (IDC) of grade 2 in her left breast. The figure demonstrates a sodium (^{23}Na) MR image reconstructed using wTV for c) 8 projections, g) 16, e) 32, and i) 64 radial projections and dTV for d) 8 projections, f) 16, k) 32, and j) 64 radial projections. k) show the image reconstructed using the AG-TV and a l) ground truth sodium image (ADC). Gray-scale bar shows image signal intensity (SI) in arbitrary units (a.u.)

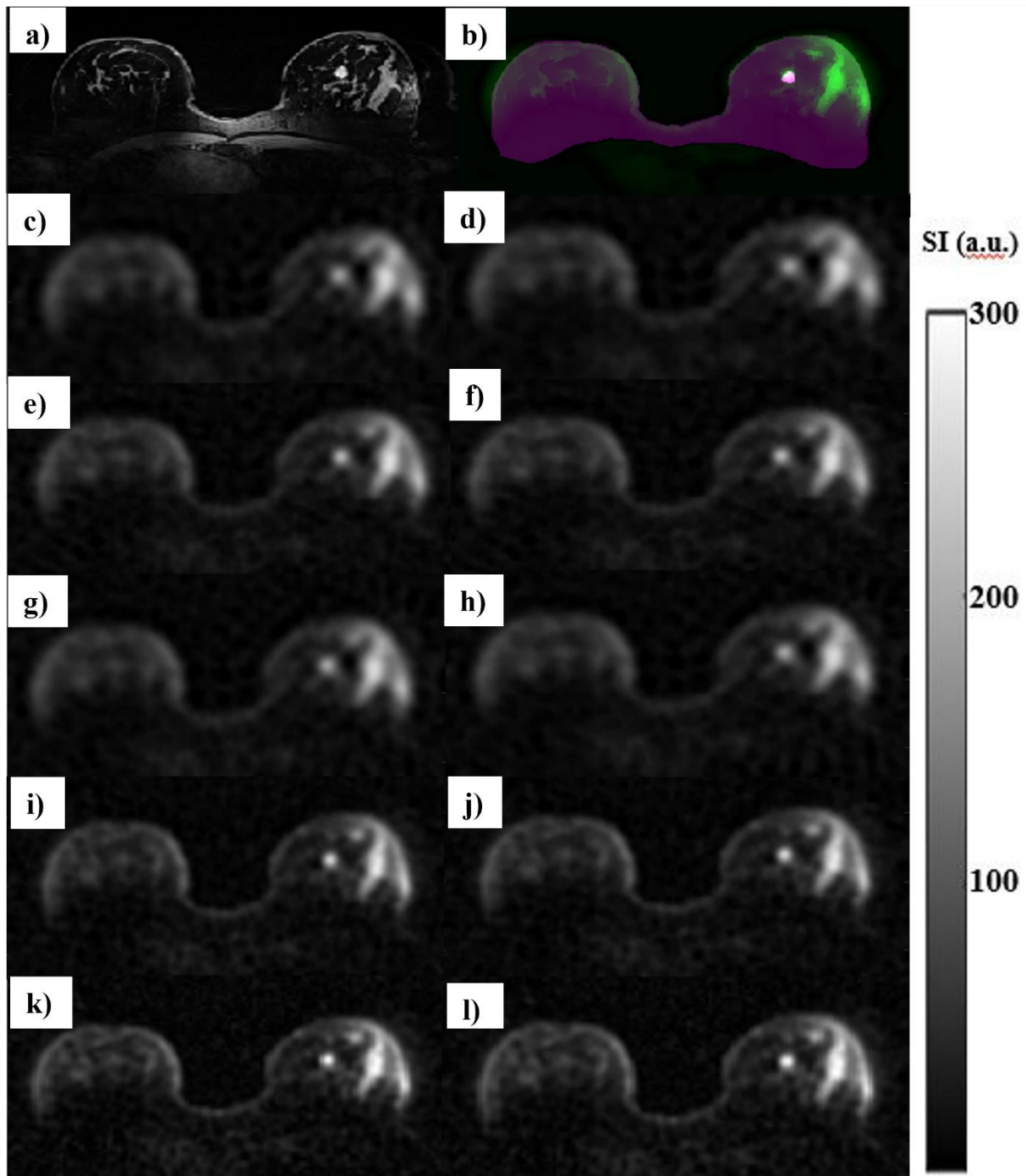


Figure 3: A 46-year-old female subject (#14) with multicentric invasive ductal carcinoma (IDC) of grade 3 in her left breast. The figure demonstrates a sodium (^{23}Na) MR image reconstructed using wTV for c) 8 projections, g) 16, e) 32, and i) 64 radial projections and dTV for d) 8 projections, f) 16, k) 32, and j) 64 radial projections. k) show the image reconstructed using the AG-TV and a l) ground truth sodium image (ADC). Gray-scale bar shows image signal intensity (SI) in arbitrary units (a.u.)

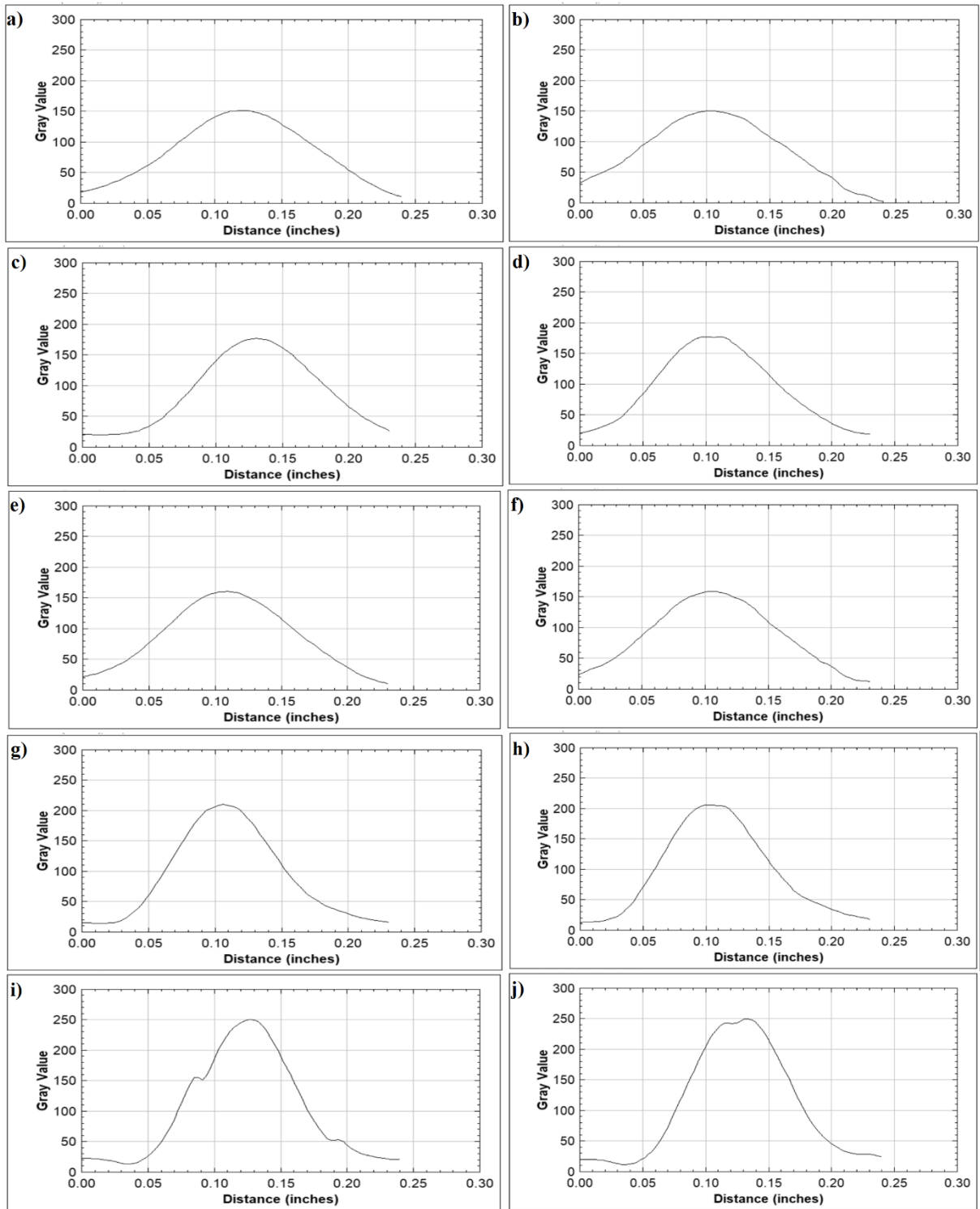


Figure 4: Graphical representation of the sodium signal intensity (SI) profiles through the tumor of the subject#14. The SI profiles were generated on ^{23}Na -MR images reconstructed using wTV for a) 8 projections, c) 16, e) 32, and g) 64 radial projections and dTV for b) 8 projections, d) 16, f) 32, and k) 64 radial projections. i) show the image reconstructed using the AG-TV and a j) ADC reconstruction.

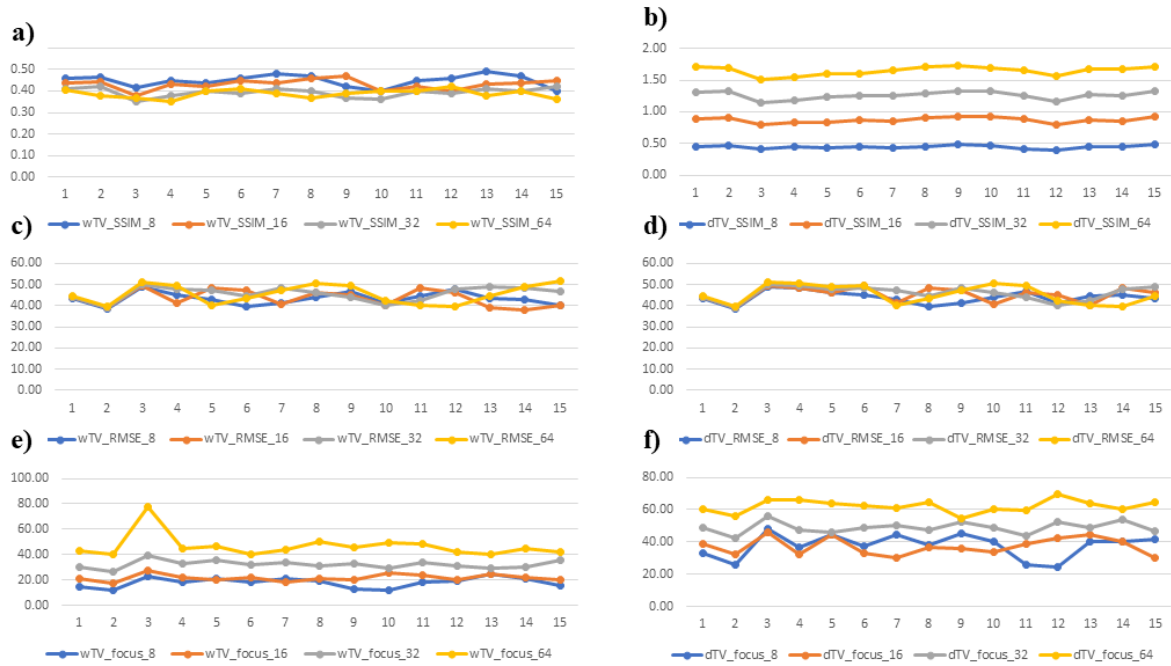


Figure 5: Demonstrated image quality metrics SSIM (structural similarity index) (a, b), RMSE (root mean square error) (c, d), and focus measure (e, f) for the Ehrhardt et al. wTV and dTV approach for the different number of radial projections (8, 16, 32, 64).

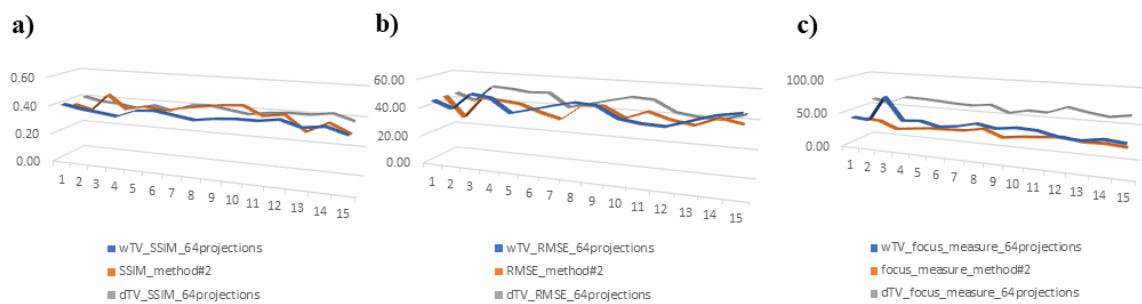


Figure 6: Graphical presentation of image quality parameters: structural similarity index (SSIM) (a), root mean square error (RMSE) (b), and focus measure (c) obtained using wTV, dTV methods and the method by Licht et al. (method#2)

Acknowledgment:

Conflict of interest statement:

The authors declare that they have no known competing financial interests or personal relationships that could have appeared to influence the work reported in this paper.